Desalination and Water Treatment
www.deswater.com

doi: 10.5004/dwt.2018.22351

114 (2018) 320–331
May

Synthesis and characterization of rGO/Co_3O_4 composite as nanoadsorbent for Rhodamine 6G dye removal

Salam H. Alwan Altaa*, Hassan A. Habeeb Alshamsi, Layth S. Jasim Al-Hayder

Department of Chemistry, College of Education, University of Al-Qadisiyah, Diwaniya 1753, Iraq, Tel. +9647808163781; email: salamhussein354@gmail.com (S.H.A. Altaa), Tel. +9647827626352; email: hasanchem70@gmail.com (H.A.H. Alshamsi), Tel. +9647702526593; email: layth.alhayder@gmail.com (L.S.J. Al-Hayder)

Received 30 December 2017; Accepted 7 April 2018

ABSTRACT

In this paper, Co_3O_4 nanoparticles are loaded onto rGO sheet by the hydrothermal method and used as a surface to absorb the cationic dye (Rhodamine 6G). They are characterized using X-ray diffraction, field emission scanning electron microscopy, transition electronic microscopy, UV-Vis spectroscopy, Fourier transform infrared spectroscopy, energy dispersion X-ray, and zeta potential. The results indicated that there was heterogeneous distribution of Co_3O_4 nanoparticles (45 nm in size) on rGO sheets. The rGO/Co_3O_4 nanocomposite showed adsorption capacity with 122.4 mg/g for Rh.6G dye. Additionally, the factors affecting the process of adsorption that include equilibrium time, temperature, pH solution, ionic intensity, and adsorbent dose were studied. The equilibrium removal efficiency was studied using Langmuir, Freundlich, and Temkin isotherm models. The kinetic data were analyzed with two different kinetic models and pseudo-first-order kinetic model was found to be the best model for our adsorption experiment. The thermodynamic parameters including Gibbs free energy ($\Delta G°$), standard enthalpy change ($\Delta H°$), and standard entropy change ($\Delta S°$) were calculated for the adsorption process.

Keywords: Adsorption; Graphene oxide; Kinetic; Nanocomposite; Rhodamine 6G

1. Introduction

Presently, water pollution with dyes has become an environmental problem that adversely affects human health. Dyes are the most common contaminants available in wastewater [1]. Many industries produce dyes, for example, textiles, paper, plastics, leather, food, and cosmetics. [2]. In addition, dyes pose a deadly hazard to humans because of its bioaccumulation properties. Therefore, the processes for treatment of dye wastewater have made many researchers interested in this area and the use of various techniques to reduce that problem [3]. To eliminate contamination problem with dyes, scientists resort to use various techniques, for example, adsorption, coagulation [4], chemical oxidation [5], membrane filtration [6], ion exchange [7], and photocatalysis [8]. Adsorption is one of the best prominent technologies mentioned above in water treatment because it is highly efficient, easy to operate, and cost effective [9]. After the invention of graphene, its application was not only in electronic and energy industry, but also in the scope of environmental remediation [10,11]. Graphene single-layer material of the carbon allotropes possesses a two-dimensional lattice form of C atoms with sp^2 hybridization. The reason for the usage of graphene is often due to its excellent properties such as great surface area, which provides good adsorption capacity and good mechanical strength, an outstanding thermal stability, and excellent optical and electrical properties [12]. After the treatment of the graphite, using strong oxidizing factors according to the modified Hummer's method, graphene oxide (GO) was produced [13]. The process showed the introduction of functional oxygen groups such as hydroxyl, epoxy, and carboxyl on the surface of the graphite and then dispersing the layers using ultrasonication. It was

* Corresponding author.

observed that the oxygen-containing groups were able to form chemical bonds with the dyes to be suitable for final removal of dyes from wastewater, etc. [14]. GO is an excellent precursor of reduced graphene oxide (rGO) that can be found using green reduction of exfoliated GO. Furthermore, the remaining oxygen-containing groups allow the addition of chemical modifications on the rGO surface [15]. It has been recently reported that graphene incorporated with nanoparticles, such as TiO_2 [16], Co_3O_4 [17], SnO_2 [18], and ZnO [19], show high activities in adsorption, electrochemical catalysis, capacitors, photocatalytic degradation, etc. Since rGO hybrids can exhibit enhanced performance, it has become a priority for researchers to prepare these nanocomposites. Among the reported transition metal oxides, the cobalt(II, III) oxide (Co_3O_4) has delivered the promising electrochemical performance as an anode material for lithium-ion batteries [20] and superior specific capacitance for supercapacitors [21]. The synthesis of nanocrystalline Co_3O_4 has been carried out with various methods to obtain nanosize Co_3O_4 of different designs, such as nanotubes [20], nanoparticles [22], nanorods [23], and hollowed spheres [24]. To raise the efficiency of the adsorbent materials, rGO papers should be decorated with Co_3O_4 nanoparticles to give a composite form that possesses wonderful properties, for example, high conductivity, great surface area, speedy electronic transfers, excellent mechanical flexibility, and good chemical stability [25,26]. The process of loading nanoparticles on the rGO sheet also prevents the conglomeration of individual nanopapers and nanomaterials [27]. The previous research in this regard has shown rather effective results. Encouraged by these studies efforts have been made to prepare rGO/Co_3O_4 nanocomposite [28–31].

In this paper, the rGO/Co_3O_4 nanocomposite was prepared and used to remove Rhodamine 6G dye from the contaminated water. Batch studies were performed by varying the contact time, temperature, pH solution, and ionic intensity. The following is a description of the characterization of rGO/Co_3O_4 nanocomposite using various techniques listed below to define the nanosize, thermal stability, and determining the quality of active groups.

2. Materials and methods

2.1. Chemicals

Graphite precipitate, 97% H_2SO_4, 37% HCl, H_3PO_4, NaOH, and ethanol were obtained from BDH Company, Republic of India and used directly without primary purification. 30% H_2O_2, NaCl, and NaOH were supplied from Scharlau, Barcelona, Spain. $KMnO_4$ and $NaNO_3$ were supplied from Merck, Kenilworth, USA. Rhodamine 6G was obtained from chem-supply, Australia. Ascorbic acid, l-tryptophan, $CoCl_2$, and $CoNO_2$ were supplied from BDH Company. Deionized (DI) water was used as the solvent in all the experiments.

2.2. Instruments

The crystalline character of the solid has been identified by X-ray diffraction (XRD) analysis using a D/Max 2,550 V diffractometer with Cu Kα radiation (λ = 1.54056 Å) (Rigaku, Tokyo, Japan), and the 60 XRD data were collected at a scanning rate of 0.03 s^{-1} for 2θ in a range from 5° to 80°. Fourier transform infrared spectroscopy (FTIR) analysis was accomplished by a Nicolet Nexus 670 FTIR instrument with KBr tablets as sample holders in the 4,000–400 cm^{-1} region. The UV-Visible tests were accomplished by Cary 300 Bio UV-Visible spectrometer in the wavelength range 200–900 nm, using 10 mm path length cuvette. The morphology of prepared materials was noted by field emission scanning electron microscopy (FE-SEM, JEOL, JSM-6701F, Japan) operated at an acceleration voltage of 8.0 kV and transmission electron microscopy (TEM) notes were performed using Joel 2100 TEM under an accelerating voltage of 200 kV. The zeta potentials of prepared materials were measured using laser Doppler electrophoresis with a Zetasizer Nano-ZS (Malvern Instruments Ltd., Worcestershire, UK) HCl and NaOH (0.1 M) were used to regulate the acidic function.

2.3. Preparation of GO, rGO, Co_3O_4, and rGO/Co_3O_4 composites

GO was prepared by oxidation of pristine graphite powder via the improved Hummer's method [32]. The rGO was prepared by mixing 0.1 mg/mL GO with 5.0 mg/mL l-ascorbic acid as a reducing agent and l-tryptophan as a stabilizing agent with a strong base (NaOH), where the solution is mixed into the sonication bath for 30 min. After the previous step, a mixture was left under reaction at a temperature 80°C for 24 h. At the end of the time, the solution was cooled to room temperature and then returned to the sonication bath for 1 h. Then, the resulting solution was washed with DI water and separated using a centrifuge (6,000 rpm) for 10 min to obtain a black powder to guide the reduction of the GO. In the end, the powder was dried in an oven at 50°C for 1 d to get rGO nanosheets [33]. In contrast, cobalt oxide nanoparticles were prepared by the solvothermal method. The cobalt(II) nitrate ($Co(NO_3)_2{\cdot}9H_2O$) was mixed with sodium dodecyl benzene sulfonate. Such solution was dissolved in 40 mL absolute ethanol and inserted it into the sonication bath for 30 min to obtain a dark green solution. The resultant mixture is transferred into a 100 mL sealed Teflon-lined autoclave and kept at 180°C for 6 h. After cooling the autoclave to room temperature, the dark precipitate was obtained, filtered, washed with distilled water, and afterwards with absolute ethanol to eliminate any alkaline salt and surfactant that remained in the final product, and dried at 90°C for 6 h under vacuum. The obtained powder was calcined at 400°C for 3 h, and a black crystalline precipitate evidently formed Co_3O_4 nanoparticles were obtained [34,35]. Finally, rGO/Co_3O_4 nanocomposite was prepared using the hydrothermal process which involves dissolution of 0.1 g of GO in 200 mL DI distilled water by inserting it into the sonication bath for 1 h to obtain GO suspension. Then, 1.4 g cobalt chloride ($CoCl_2{\cdot}6H_2O$) was dissolved in 10 mL of water and then the mixture was stirred for 2 h to complete the ion exchange process. After that, 10 mL sodium hydroxide (1 equivalent) in the form of drops was added with the solution stirred for 1 h. 1.5 mL of 30% H_2O_2 was added to the mixture, inserted it into the Teflon-lined stainless steel autoclave and heated at 100°C for 4 h. Next, 0.25 g of reduced agent l-ascorbic acid was added and transferred into autoclave, heated again at 120°C for 4 h. The powder yield was collected by a centrifugal method, washed with DI water, and then dried to obtain black powder rGO/Co_3O_4 nanocomposite calcined at 150°C for 4 h [36].

2.4. Adsorption experiments

2.4.1. Batch adsorption experiments

The stock solution of 100 mg/L Rh.6G solution was prepared by dissolving 0.1 g Rh.6G powder in 100 mL of water. An aqueous solution (10 mL) with 1 mg nanocomposite and a suitable concentration of Rh.6G was shaken by a thermostatic reciprocating shaker at 120 rpm at 25°C. After removal of the nanocomposite by filtration through a centrifuge of 6,000 rpm, the dye concentrations in the supernatant were determined by a UV-Visible spectrophotometer.

The adsorption capacity (q_t, mg/g) and the removal percentage (%) were calculated from the following equation [37]:

$$q_t = \frac{V_{sol.}(C_o - C_e)}{m} \quad (1)$$

$$\text{Removal } \% = \frac{(C_o - C_e)}{C_o} \times 100 \quad (2)$$

where C_o and C_e are the initial and final concentrations of dye in the solution (mg/L), respectively, V is the volume of the solution (mL), and m is the mass of nanocomposite (mg).

2.4.2. Effect of adsorbent dose

The effect of surface mass (rGO/Co_3O_4) on the process of adsorption of the dyes was studied using different weights (0.001, 0.002, 0.003, 0.06, and 0.01 g) per 10 mL of dye solution. This factor requires the stabilization of all conditions (dye concentration, temperature, and acid function). The dye solution was mixed with the adsorbent surface and placed in a water bath shaker for 6 h. The samples were then centrifuged at a speed of 6,000 rpm to remove the adsorbent and the residual dye concentration was measured using a UV-Vis spectrophotometer.

2.4.3. Effect of temperature

The adsorption procedure was repeated in the same manner at temperatures of 10°C, 20°C, 30°C, and 35°C in a range of concentrations between 5 and 200 mg/L to estimate the basic thermodynamic functions.

2.4.4. Effect of pH

The effect of the acidic function was studied in the adsorption process. All conditions were stabilized at temperature 25°C and concentration 100 mg/L. The weight (0.01 g) of the nanocomposite (rGO/Co_3O_4) was used and the dye solutions were added at different pH values (2.0–12.0) and the pH values were regulated with diluted HCl and NaOH solutions (0.1 M). The pH solution at the beginning of the adsorption was measured using a pH meter. The results were presented by drawing the amount of the adsorbed substance versus the value of the acidic function and its effect on the adsorption process.

2.4.5. Effect of ionic strength

The effect of ionic strength was measured using different weights of NaCl (0.001, 0.01, 0.05, 0.1, 0.15, 0.2, 0.3, and 0.4 g). A constant concentration of dye solutions was added to volumetric flasks containing 0.01 g of the nanocomposite (rGO/Co_3O_4). Then, the solutions were agitated using a water bath shaker at 120 rpm and 25°C. When equilibrium was achieved, a centrifuge with 6,000 rpm separated the adsorbate and the residual dye concentration was measured.

3. Results and discussion

3.1. Characterization of rGO/Co_3O_4 nanocomposite

Fig. 1 shows the XRD pattern of pure graphite displaying a sharp peak at 2θ ≈ 26.5°, which corresponds to *d*-spacing of 3.36 Å. After oxidation process, the formation of GO shows the appearance of a new peak, which is a diffraction peak at around 11.6 Å, which corresponds to an interlayer *d*-spacing of 7.60 Å. The rGO displays a broad diffraction peak at 25.7°, corresponding to an interlayer *d*-spacing of 3.49 Å [38]. In contrast, the XRD pattern of Co_3O_4 nanoparticles displays the diffraction peaks (2θ = 19.09°, 31.35°, 36.92°, 38.62°, 44.87°, 55.71°, 59.42°, and 65.30°). All diffraction peaks of cobalt oxide can be indicated to cubic spinel Co_3O_4 crystal phase. The very sharp diffraction peaks and high intensity propose the high crystallization of the Co_3O_4 nanoparticles. The XRD pattern of rGO/Co_3O_4 nanocomposite displays diffraction peaks at 2θ = 19.03°, 31.63°, 36.71°, 38.51°, 45.34°, 56.36°, 59.34°, and 65.07° indicating the cubic spinel Co_3O_4. An additional small broad diffraction peak displaying at 2θ = 24.5°–29.5° corresponding to the irregular accumulate graphene sheets, while the diffraction peak of GO sheet approximately disappeared. The peak positions can be completely indicated to the face-centered cubic [39].

Fig. 2 shows the FTIR spectrum of pristine graphite which has two peaks at approximately 1,668 cm^{-1} due to the skeletal vibration from graphite field (the sp^2 aromatic C=C) and a vibration band at 3,444 cm^{-1} probably related to adsorbed water molecules. After oxidation process, O–H stretching vibrations (3,100–3,500 cm^{-1}), alkoxy stretching vibrations (1,040–1,170 cm^{-1}), O–H (C–O) distortion peaks (1,300–1,400 cm^{-1}), and the stretching vibration of epoxy

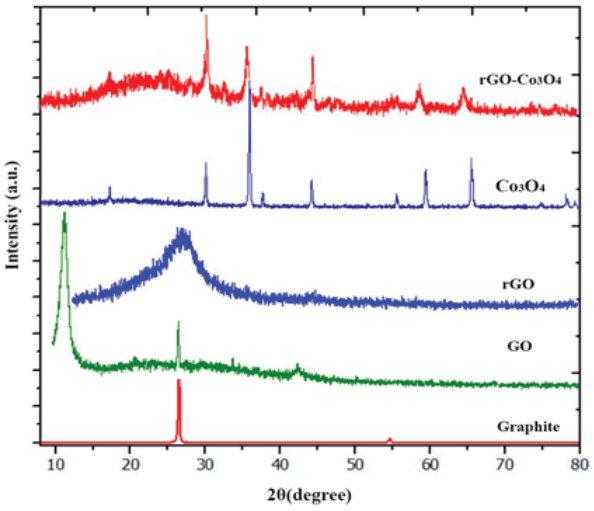

Fig. 1. XRD spectra of Gr, GO, rGO, Co_3O_4, and rGO/Co_3O_4.

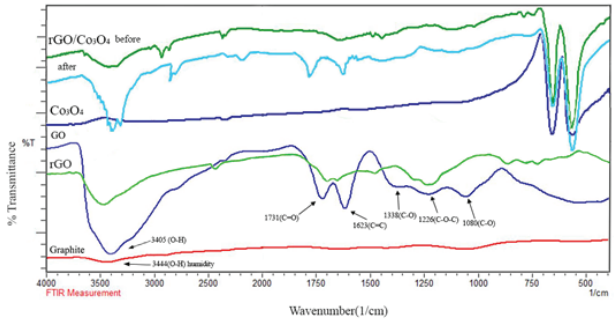

Fig. 2. FTIR analysis of G, GO, rGO, Co_3O_4, and rGO/Co_3O_4 before and after adsorption.

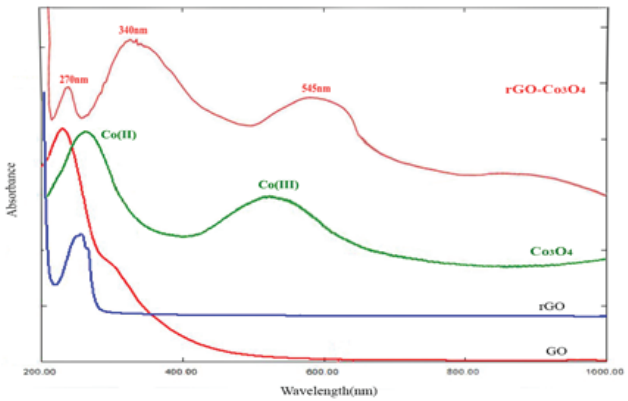

Fig. 3. UV-Vis analysis of GO, rGO, Co_3O_4, and rGO-Co_3O_4.

(C–O–O) groups (1,000–1,280 cm^{-1}) appeared. Significantly, the aromatic C=C peak could be identified between 1,600 and 1,650 cm^{-1}. After reducing with ascorbic acid, the peak at 1,700, 1,330, and 1,226 cm^{-1} almost disappears and the peak for OH stretching bonds at 3,490 cm^{-1} weakens obviously. This evidently proves the effective removal of oxygen from the sheets. Furthermore, it exhibits new band in the region of 2,410 cm^{-1} associated to the presence of $–CH_2$ stretching vibrations [40]. In contrast, FTIR spectrum of Co_3O_4 nanoparticles before adsorption shows two strong absorption bands at 663.4 and 570.8 cm^{-1}. This proves the formation of the spinel network of Co_3O_4, while rGO/Co_3O_4 composite displays strong absorption bands at 663.4 and 570.8 cm^{-1} are attributed to the presence of Co_3O_4. It was observed that these functional groups were almost removed through the way of thermal treatments, and thus the GO is transformed into rGO. Furthermore, an appearance of a new absorption band at about 1,511 cm^{-1} may be attributed to the skeletal vibration of the rGO sheets. After Rh.6G dye adsorption, there is remarkable shift in the positions of –OH, C=O group peaks. Fig. 2 also exhibits the characteristic stretching peaks of saturated C–H(CH_3) at 2,932 cm^{-1}, stretching vibration of C–N at 2,338 cm^{-1} and the peak related to the vibration of the aromatic ring at 1,600 cm^{-1} is very prominent, which showed that the Rh.6G has been anchored on the surface of adsorbent after the adsorption. It is worth nothing that the carboxyl (C=O) peak shifted to 1,719 cm^{-1} in Fig. 2, due to the reaction between carboxyl functional groups and Rh.6G. This can be explained by the following reason: Rh.6G is a kind of cationic dye, which can be adsorbed easily by electrostatic forces on negatively charged surfaces [38,41].

The absorption spectrum of GO in Fig. 3 shows two absorption peaks at 229 nm which can be returned to the π–π^* transition of aromatic (C=C) bonds and at 300 nm associated to the n–π^* transition of the carbonyl groups (C=O) bonds. The rGO obtained the red shift up to 280 nm owing to the restoration of the sp^2 hybridized carbon grid due to the removal of the oxygen bearing functional groups [42,43]. UV-Vis spectra of the Co_3O_4 nanoparticles show two wide absorption peaks in the wavelength ranges of 230–380 and 420–630 nm can be attributed to the formation of cobalt oxide. In contrast, UV-Vis spectra of the rGO–Co_3O_4 nanocomposite contain three peaks. The two peaks at the wavelength 340 and 545 nm assigned Co_3O_4 nanoparticles and the absorption peak at 270 nm attributed to π–π^* transitions of the aromatic C=C of rGO sheet [44,45].

The morphologies of the prepared nanomaterials were studied by FE-SEM and TEM. Fig. 4 shows FE-SEM analysis of GO nanosheets tend to congregate together to form multilayer agglomerates. The individual nanosheets have sizes extending from tens to several hundreds of square nanometers [46]. However, reduced GO had a wrinkled paper-like morphology with severely folded lines [47]. The FE-SEM image of Co_3O_4 nanoparticles shows a sphere-like morphology and is composed of agglomerated assembled spheres indicate a uniform homogeneity and good connectivity between the nanoparticles [48].

The surface morphology of the nanocomposite before and after Rh.6G dye adsorption was observed using FE-SEM analysis. There are significant changes to the surface morphology of the nanocomposites, as well as the formation of discrete aggregates on their surfaces following Rh.6G dye adsorption. The FE-SEM image of rGO/Co_3O_4 nanocomposite before adsorption shows rough surface and Co_3O_4 distributed as bright dots uniformly on the surface of the rGO nanosheets. These observations demonstrate the presence of both rGO and Co_3O_4. After Rh.6G dye adsorption as presented in Fig. 4, nanocomposite displayed a dense and porous surface texture. Interaction of rGO/Co_3O_4 with Rh.6G dye has resulted in the formation of flake-like deposits on its surface [15].

The EDX analysis and the elemental maps show that the prepared rGO/Co_3O_4 composite includes only cobalt, carbon, and oxygen, similar to the chemical composition of the nanocomposite. The appearance of the carbon signal in the spectrum is associated to the rGO network (Fig. 4). After Rh.6G dye adsorption a new peak appeared assigned to present nitrogen.

TEM analysis can be used to identify the morphology of prepared nanoparticles by passing a beam of electrons through the sample to give a picture on a phosphor screen, so that it can be different from SEM [49]. TEM image of GO shows silk waves, transparent and exhibit a very stable nature under the electron beam [50]. TEM image of the rGO sheet demonstrates a wrinkled paper-like structure. This is due to the chemical bonding of carbon atoms in either a single layer or multilayers [51]. TEM image of Co_3O_4 nanoparticles explains semispherical, porous texture, a uniform distribution, and very homogeneous surface [52]. TEM image of rGO/Co_3O_4 nanocomposite displays uniform size

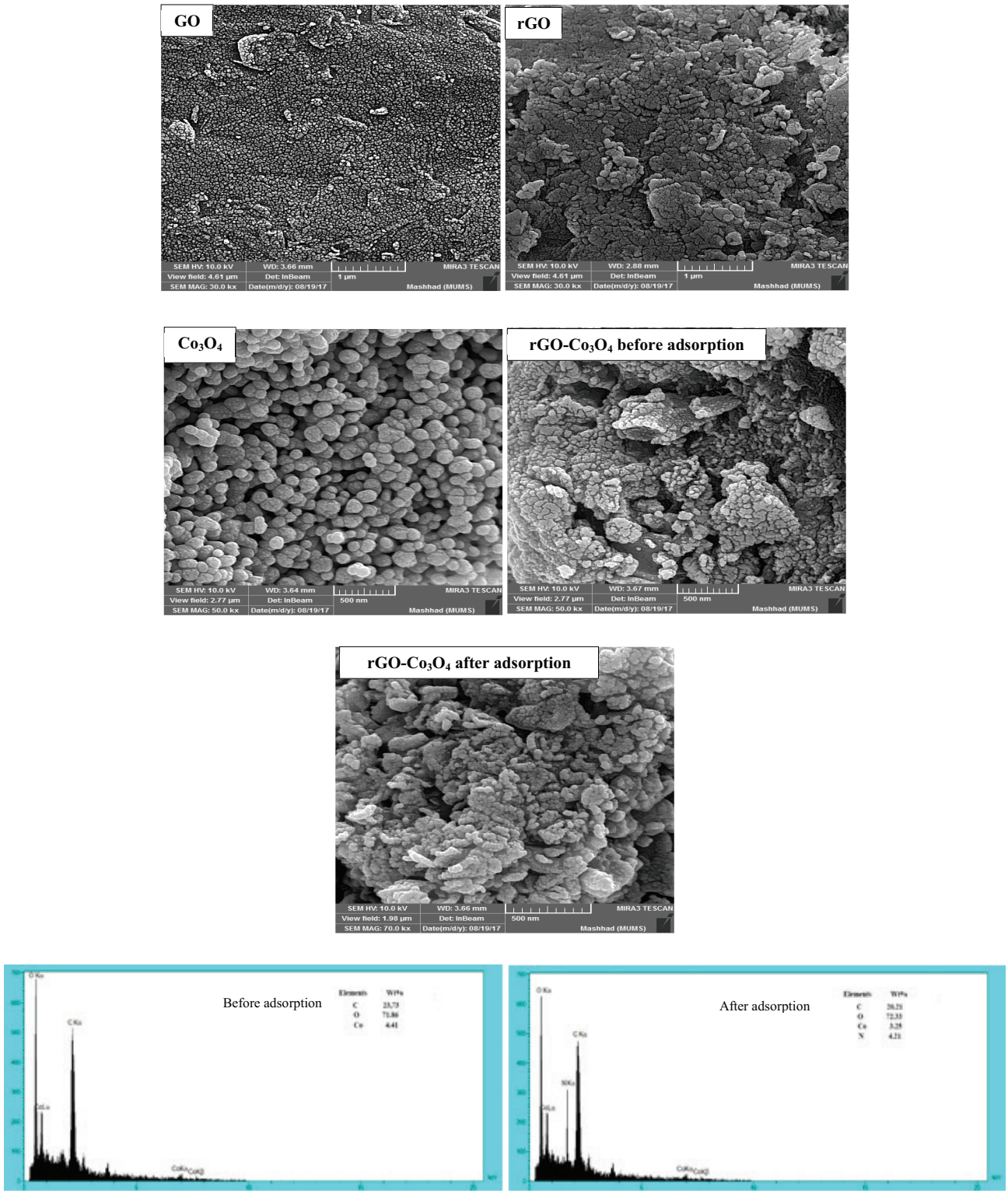

Fig. 4. FE-SEM analysis of GO, rGO, Co_3O_4, and rGO/Co_3O_4; and EDX analysis of rGO/Co_3O_4 before and after adsorption.

of spindle-like Co_3O_4 nanoparticles distributed in a homogeneous and dense manner on rGO surface. The inclusion of Co_3O_4 nanoparticles between the interlayers of the graphene nanosheets was observed, suggesting a relatively strong interaction between rGO and Co_3O_4 particles. This prevents accumulation of the Co_3O_4 nanoparticles through thermal treatment (Fig. 5) [53,54].

The zeta potential is a physical property exhibited by any material in dispersion and is an important parameter used for characterizing the electrical properties of interfacial

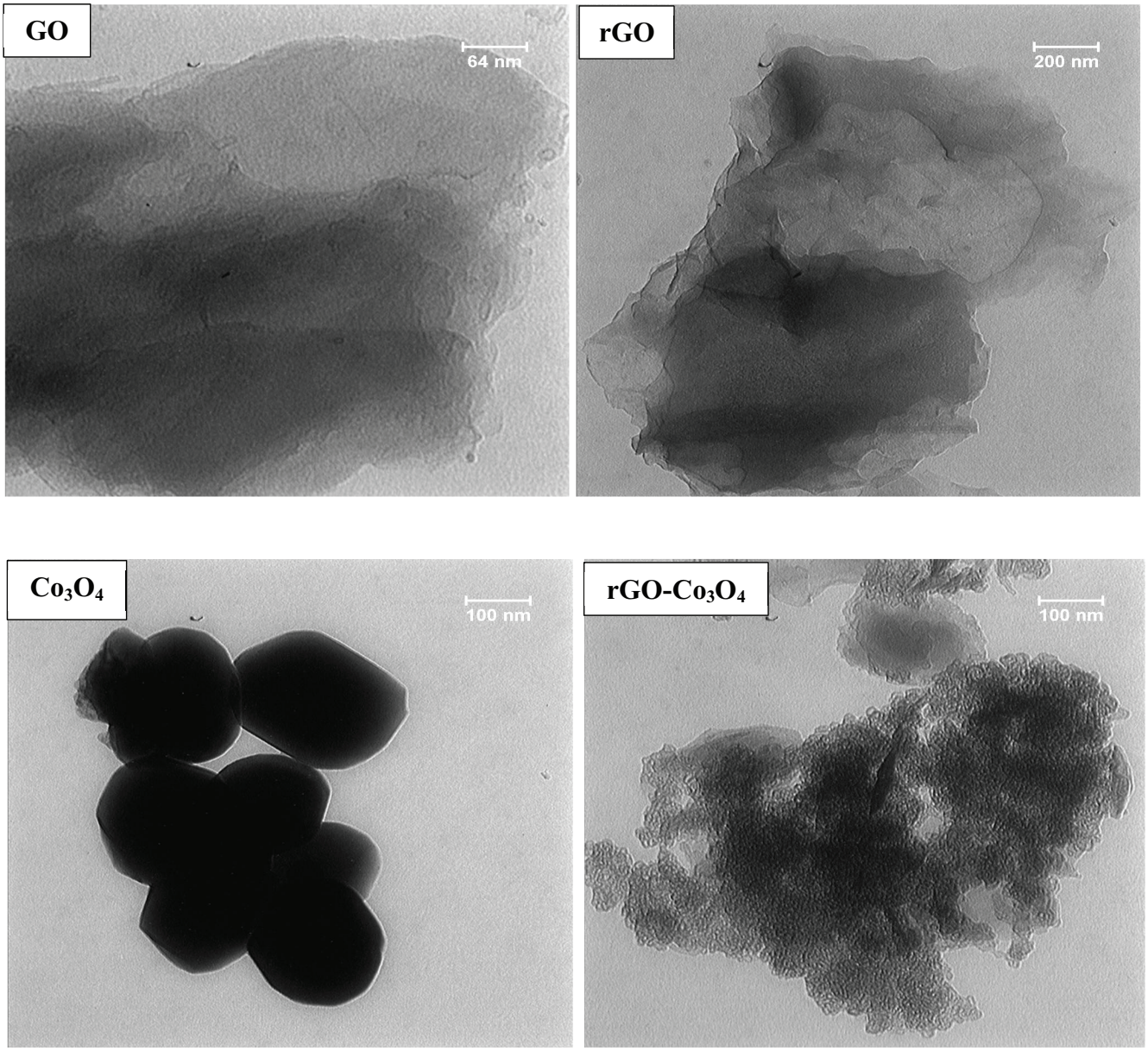

Fig. 5. TEM analysis of GO, rGO, Co_3O_4, and rGO/Co_3O_4.

layers in suspension. The GO solution would be stabilized when the zeta potential value becomes −46 mV in the pH range of 9–12 (Fig. 6). The negative zeta potential value of GO is due to the presence of electronegative functional groups formed at the graphite lattice during the oxidation [55]. Zeta potential of rGO solution is up to +8.85 mV. The positive zeta potential values of rGO at pH <5 are attributed to adsorption of positively charged ions (e.g., H^+ and Na^+) in the aqueous solution [56]. Zeta potential of Co_3O_4 solution up to +23.1 mV is attributed to the surface of the metal oxide is more positive and this leads to electrostatic interference between the metal and the rGO network. Finally, the zeta potential of the rGO/Co_3O_4 nanocomposite around −48.8 mV shows that the surface of the composite is more stable in the

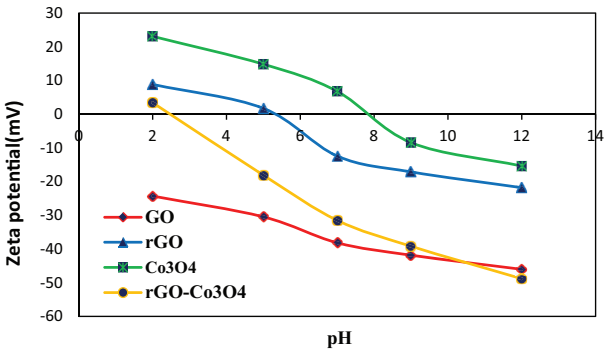

Fig. 6. Zeta potential of GO, rGO, Co_3O_4, and rGO/Co_3O_4.

alkaline medium and has a negative charge that can directly attract the cationic dye [57].

The specific surface area is calculated by employing the Brunauer–Emmett–Teller (BET) method and the pore size distributions are obtained by means of the Barrett–Joyner–Halenda (BJH) method equation using the adsorption isotherm branch, which are shown in Fig. 7. The BET specific surface area and the pore diameter of rGO/Co_3O_4 nanocomposite before adsorption were found to be 82.202 m^2/g and 4.61 nm, respectively. The value of the pore diameter suggested that rGO/Co_3O_4 nanocomposite was a mesoporous material. The isotherms exhibit a typical type-V shaped curve and a H2 hysteresis loop at a relative pressure of 0.98, indicating the presence of slit-shaped pores between the parallel layers of nanocomposite. After Rh.6G dye adsorption, the specific surface area and the pore diameter of nanocomposite are 41.296 m^2/g and 2.71 nm, respectively. The results show a significant decrease in the surface area after Rh.6G dye adsorption as shown in Table 1. This indicates an interaction between dye and nanocomposite [58].

3.2. Adsorption experiments

3.2.1. Effect of adsorbent dosage

An adsorption experiment of Rhodamine 6G dye removal is performed using different weights (0.001–0.01 g) of the nanocomposite. Note that dye increases the removal percentage with increasing weight of the nanocomposite. This can be attributed to the greater surface area of nanocomposite and the increase in the available active sites for Rh.6G dye adsorption. Consequently, the uptake of Rh.6G reaches a saturation level at 0.01 g nanocomposite as the active sites present on the surface of rGO/Co_3O_4 become saturated with Rh.6G. For subsequent experiments, 0.01 g of sorbent dose was selected (Fig. 8(a)) [59].

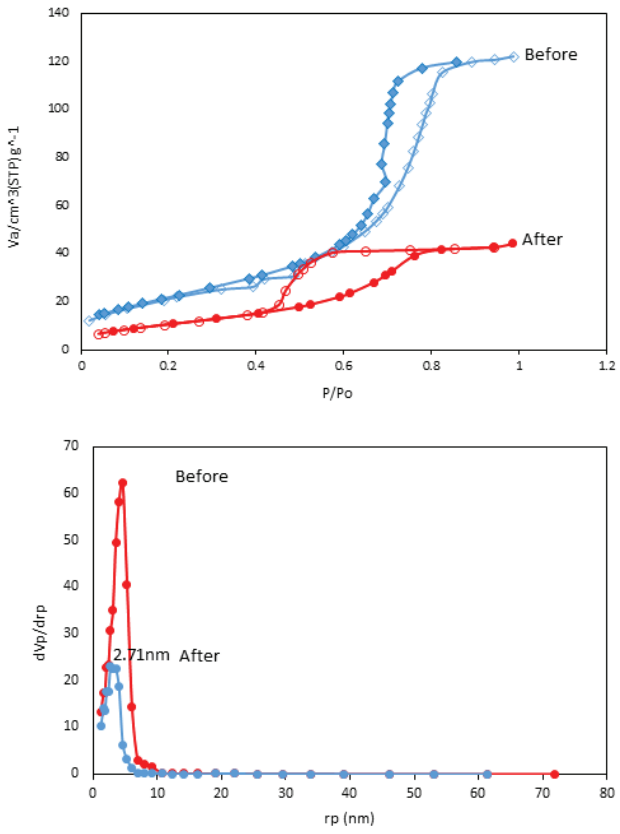

Fig. 7. N_2 adsorption and desorption curves and pore size distributions of rGO/Co_3O_4 before and after adsorption.

3.2.2. Effect of contact time and kinetics of adsorption

The study of adsorption dye at different times (1–600 min) after the stabilization of all conditions affecting. In Rhodamine 6G dye adsorption capacity was increased with increasing the time to its maximum value (saturation state) but sometimes the adsorption capacity decreases with increasing time due to a desorption process (Fig. 8(b)) [60].

In order to investigate the mechanism of adsorption and potential rate controlling steps, two kinetic models, namely, pseudo-first-order and pseudo-second-order equation models were analyzed. The pseudo-first-order equation is expressed as follows:

$$\log\left(q_e - q_t\right) = \log q_e - \frac{k_1}{2.303}t \tag{3}$$

where k_1 is the rate constant of adsorption (min^{-1}). The plot of log ($q_e - q_t$) against t gives a linear relationship from which k_1 and q_e are determined from the slope and intercept of the plot, respectively.

The pseudo-second-order model can be represented by the following linear form:

$$\frac{t}{q_t} = \frac{1}{k_2 q_e^{\,2}} + \left(\frac{1}{q_e}\right)t \tag{4}$$

where k_2 is the pseudo-second-order rate constant of adsorption (g/mg min). The values of q_e and k_2 are determined from the slope and intercept of the plot t/q_t against t.

The validity of each kinetic model was checked by the fitted straight lines and depicted in Fig. 9. The corresponding kinetic parameters and the correlation coefficients are summarized in Table 2. The value of the correlation coefficient obtained from the linear plot of pseudo-second-order model is $R^2 = 0.614$, suggesting that the applicability of this model to the adsorption processes of Rh.6G adsorption by the nanocomposite is unfeasible. The high R^2 value is obtained for pseudo-first-order model, indicating that the experimental data are well described by pseudo-first-order model.

Table 1
The specific surface areas, average pore diameters (BJH), and total pore volumes of rGO/Co_3O_4 nanocomposite before and after adsorption samples

Samples	Specific surface area (m^2/g)	Pore diameter (nm)	Total pore volume (cm^3/g)
Before	82.202	4.61	0.188
After	41.296	2.71	0.068

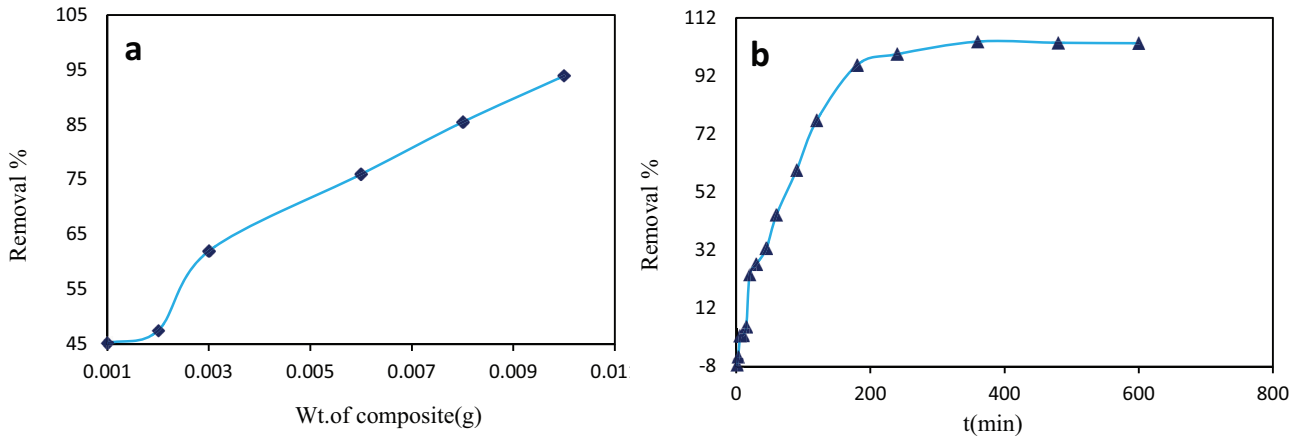

Fig. 8. Effect of (a) adsorbent dose and (b) reaction time on the removal percentage of Rh.6G dye.

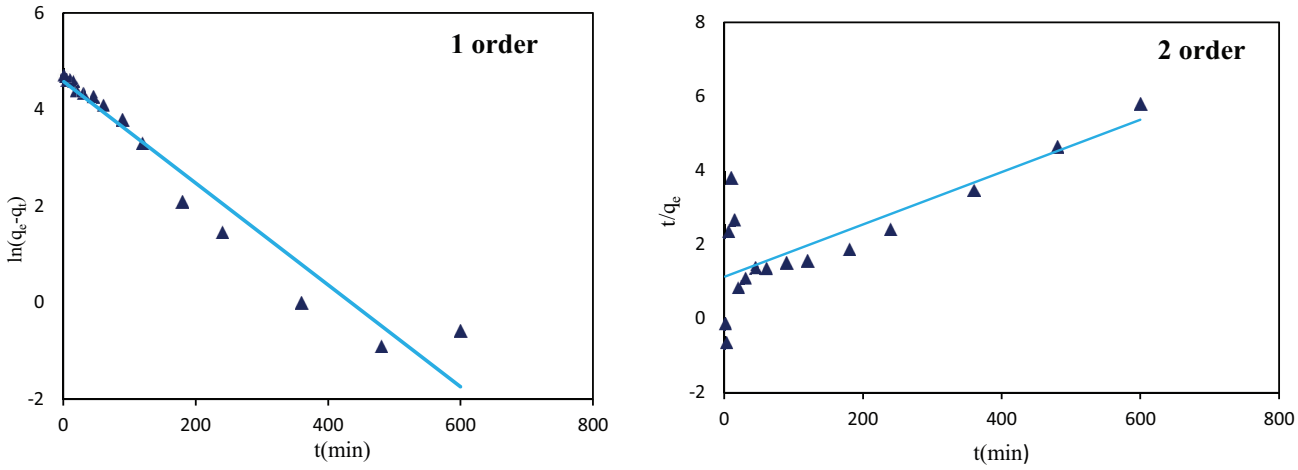

Fig. 9. Pseudo-first-order and pseudo-second-order kinetics for adsorption of Rh.6G dye.

Table 2
Adsorption kinetics parameters of adsorption of Rh.6G

Dye	Pseudo-first order			Pseudo-second order			
	k_1	q_e	R^2	k_2	q_e	h	R^2
Rh.6G	0.0105	97.582	0.950	4.467	140.845	0.886	0.614

3.2.3. Effect of pH

The pH of the aqueous solution is an important factor to affect the dye adsorption process through changing the surface charge of an adsorbent and the ionization behavior of adsorbent and dye. The influence of the solution pH on Rh.6G removal by the rGO/Co_3O_4 is shown in Fig. 10. It can be seen that the dye removal efficiencies by the nanocomposite increase with increasing pH in pH range of 2.0–12.0. The observed lower adsorption capacity at lower pH value could be attributed to the protons competition with the cationic Rh.6G for the available adsorption sites on the rGO/Co_3O_4

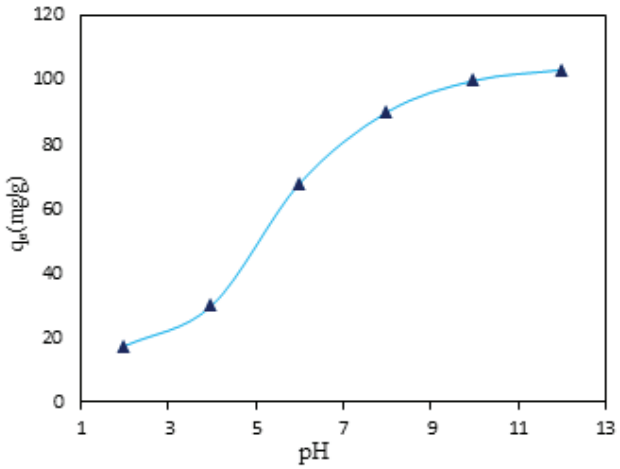

Fig. 10. Effect of pH solution on adsorption Rh.6G dye on nanocomposite.

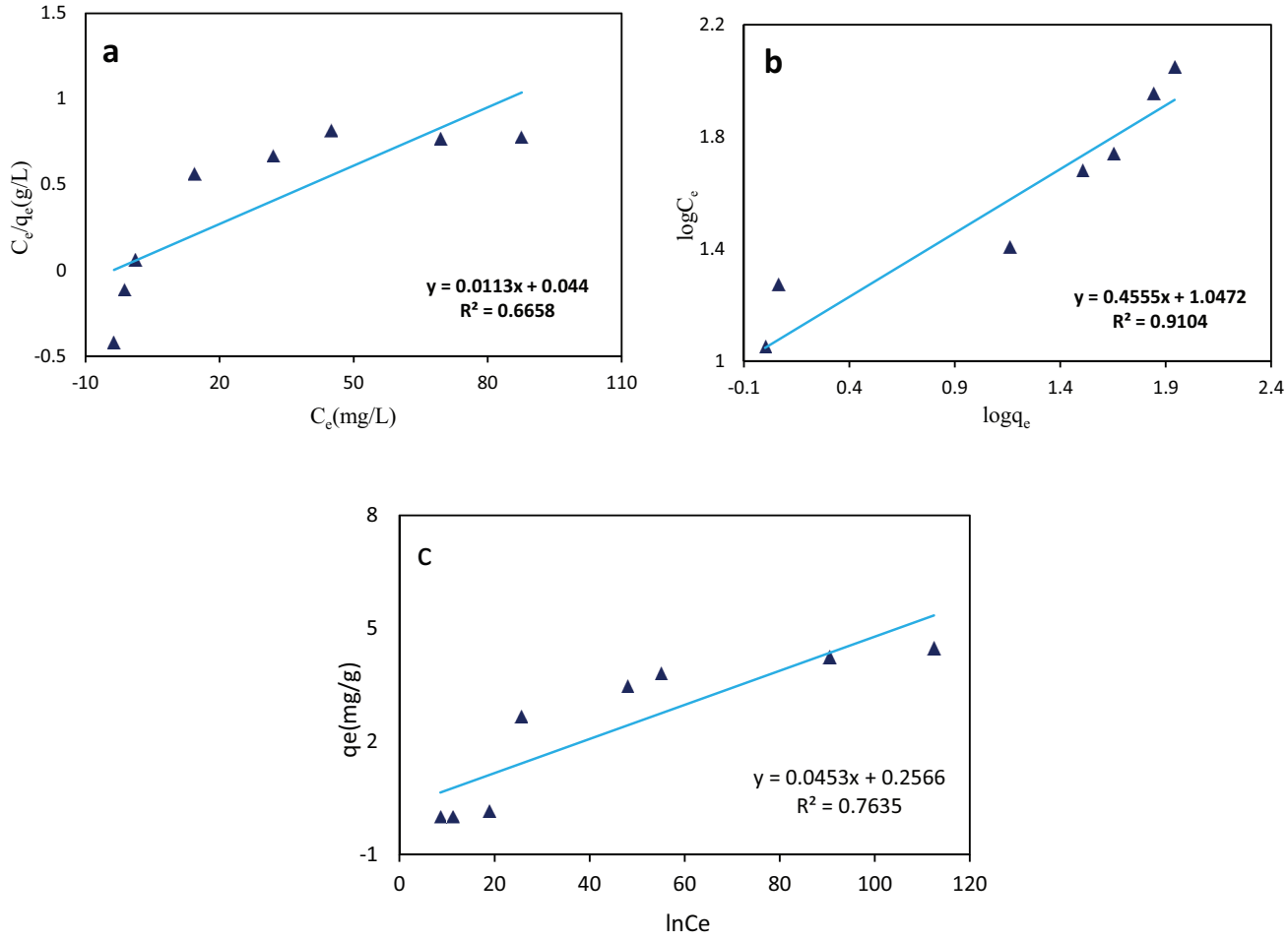

Fig. 11. Linearized form of (a) Langmuir model, (b) Freundlich model, and (c) Temkin model of Rh.6G dye.

surface. However, the surface of the rGO/Co_3O_4 may get negatively charged when the pH value increases to a certain extent. The electrostatic attraction between the negatively charged rGO/Co_3O_4 and the Rh.6G cation would lead to the increase in adsorption capacity [61].

3.2.4. Adsorption isotherm models

Three classic adsorption models, Langmuir, Freundlich, and Temkin, were used to describe the adsorption equilibrium. The mathematical representations of the Langmuir, Freundlich, and Temkin models are given below:

$$\frac{C_e}{q_e} = \frac{C_e}{q_m} + \frac{1}{K_L q_m} \tag{5}$$

$$\log q_e = \log K_F + \frac{1}{n}\log C_e \tag{6}$$

$$q_e = B\ln K_T + B\ln C_e \tag{7}$$

where q_m is the theoretical maximum adsorption capacity per unit weight of the adsorbent (mg/g), K_L, K_F, and K_T are adsorption constants of Langmuir, Freundlich, and Temkin models, respectively, and n is the Freundlich linearity index. Langmuir model is an ideal model, which possesses perfect adsorbent surface and monolayer molecule adsorption. As an empirical model, Freundlich model is widely used in the field of chemistry. Temkin model is a proper model for the chemical adsorption based on the strong electrostatic interaction between positive and negative charges [62].

The results of fitting of these models are shown in Fig. 11 and the suitable parameters for Rh.6G dye are listed in Table 3. The lower correlation coefficients R^2 of the Langmuir and Temkin point out that the isotherm data do not fit the Langmuir and Temkin models. The higher correlation coefficient R^2 = 0.910 of the Freundlich model points out that the Freundlich equation can be used to fit the experimental adsorption data and evaluate the maximum dye adsorption capacity of the nanocomposite. The results suggest that the adsorption of Rh.6G by the nanocomposite takes place in a multilayer adsorption behavior.

Table 3
Langmuir, Freundlich, and Temkin isotherm constants for Rh.6G dye uptake by rGO/Co_3O_4 nanocomposite

Dye	Langmuir equation			Freundlich equation			Temkin equation		
	K_L	q_m	R^2	K_F	n	R^2	K_T	B	R^2
Rh.6G	0.256	88.495	0.665	11.148	2.195	0.910	288.43	0.045	0.763

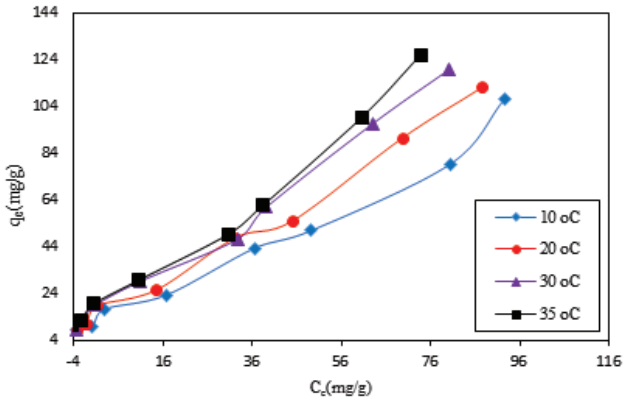

Fig. 12. Effect of temperature on the adsorption capacity of Rh.6G dye.

3.2.5. Effect of temperature and thermodynamic study

Temperature is a very important parameter controlling the adsorption process. It can modify the equilibrium capacity of the adsorbent for a particular adsorbate. Therefore, the effect of temperature on Rh.6G adsorption by rGO/Co_3O_4 was examined within a temperature range of 10°C–35°C. Fig. 12 displays the increase in removal percentage of Rh.6G with the rise in temperature. The highest removal percentage is occurring at 35°C after an equilibrium period of 360 min. Nevertheless, other increase in temperature showed a decrease in the sorption process which may have resulted from the weakening of the physical bonds between the Rh.6G molecules and the active site of the adsorbent. The increase in removal percentage of Rh.6G with a corresponding rise in temperature may have resulted from an increase in the rate of diffusion of Rh.6G molecules neighboring the external surface and internal pores of the rGO/Co_3O_4 [63].

Thermodynamic parameters involving Gibbs free energy ($\Delta G°$), enthalpy change ($\Delta H°$), and change in entropy ($\Delta S°$) are obtained at different temperatures according to the following formulas:

$$\Delta G = -RT\ln K \tag{8}$$

$$\Delta G = \Delta H - T\Delta S \tag{9}$$

$$\Delta S = \frac{\Delta H - \Delta G}{T} \tag{10}$$

$$\ln K = \frac{\Delta S}{R} - \frac{\Delta H}{RT} \tag{11}$$

Table 4
Thermodynamic parameters of adsorption of Rh.6G

Dye	Rh.6G
ΔH (kJ/mol)	+14.468
ΔG (kJ/mol)	−1.002
ΔS (J/mol/K)	+52.800
Equilibrium constant (K)	1.509

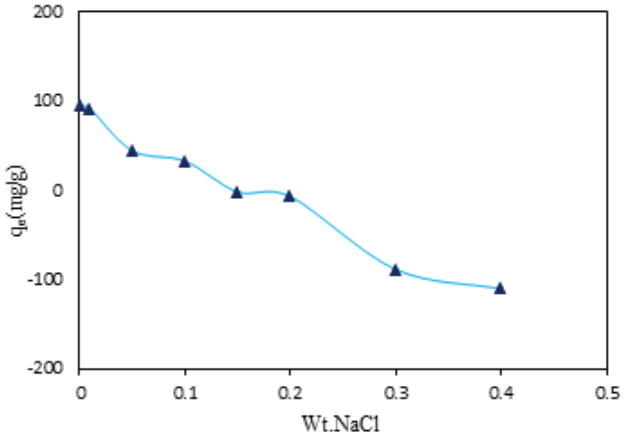

Fig. 13. Effect of ionic strength on adsorption Rh.6G dye on nanocomposite.

where R (8.314 J/mol K) is the ideal gas constant, T (K) is the absolute temperature, and k is Langmuir constant. $\Delta H°$ and $\Delta S°$ are calculated from the slope and intercept of van't Hoff plots of ln K versus T^{-1}. All these thermodynamic parameters are listed in Table 4.

The obtained value of energy $\Delta G°$ is −1.002. The negative values at three tested temperatures reveal that the adsorption process is feasible and spontaneous, and the adsorption is a physisorption and chemisorption process simultaneously. According to the positive value of $\Delta H°$, it infers that the adsorption reaction is endothermic in nature and the adsorption process is energetically stable. The positive $\Delta S°$ values suggest the increased randomness at the solid/solution interface during the adsorption process [64].

3.2.6. Effect of ionic strength

The effect of solution ionic strength on adsorption of Rh.6G by rGO/Co_3O_4 was investigated by a series of experimental studies constructed by varying weights of NaCl from 0.001 to 0.4 g. As depicted in Fig. 13, it can be seen that the adsorption capacities decrease with the addition of NaCl due

to the electrostatic repulsion effect. In previous studies, competition between Rh.6G species and Na^+ ions for the adsorbent surface decreases of the adsorption capacity [65].

4. Conclusions

In this work, rGO/Co_3O_4 nanocomposite was prepared by the hydrothermal method. This method leads to a uniform distribution of Co_3O_4 nanoparticles on rGO sheets. The rGO/Co_3O_4 nanocomposite has great potential as an effective absorbent for removing Rh.6G in aqueous solution. The morphology and XRD studies indicate that Co_3O_4 nanoparticles with a size of about 49.45 nm are homogeneously dispersed on graphene sheets. The Rh.6G adsorption follows the pseudo-first-order kinetics and the equilibrium data can be fitted well with the Freundlich isotherms. Thermodynamic parameters are calculated for the removal of dye and their values indicated that the process of removal is spontaneous and endothermic.

References

[1] P. Sharma, M.R. Das, Removal of a cationic dye from aqueous solution using graphene oxide nanosheets: investigation of adsorption parameters, J. Chem. Eng. Data, 58 (2012) 151–158.

[2] M.M. Ayad, A.A. El-Nasr, Adsorption of cationic dye (methylene blue) from water using polyaniline nanotubes base, J. Phys. Chem. C, 114 (2010) 14377–14383.

[3] C. Lijuan, Y. Jingjing, Z. Xiaopeng, Z. Lizhen, Y. Wenxia, Adsorption of methylene blue in water by reduced graphene oxide: effect of functional groups, Mater. Exp., 3 (2013) 281–290.

[4] X. Huang, X. Bo, Y. Zhao, B. Gao, Y. Wang, S. Sun, Q. Yue, Q. Li, Effects of compound bioflocculant on coagulation performance and floc properties for dye removal, Bioresour. Technol., 165 (2014) 116–121.

[5] G. Sharma, A. Kumar, M. Naushad, A. Kumar, A.H. Al-Muhtaseb, P. Dhiman, A.A. Ghfar, F.J. Stadler, M.R. Khan, Photoremediation of toxic dye from aqueous environment using monometallic and bimetallic quantum dots based nanocomposites, J. Cleaner Prod., 172 (2018) 2919–2930.

[6] A. Kumar, G. Sharma, M. Naushad, P. Singh, S. Kalia, Polyacrylamide/$Ni_{0.02}Zn_{0.98}O$ nanocomposite with high solar light photocatalytic activity and efficient adsorption capacity for toxic dye removal, Ind. Eng. Chem. Res., 53 (2014) 15549–15560.

[7] A.A. Alqadami, M. Naushad, M.A. Abdalla, M. Rizwan Khan, Z. Abdullah Alothman, Adsorptive removal of toxic dye using Fe_3O_4-TSC nanocomposite: equilibrium, kinetic, and thermodynamic studies, J. Chem. Eng. Data, 61 (2016) 3806–3813.

[8] E.M. Alrobayi, A.M. Algubili, A.M. Aljeboree, A.F. Alkaim, F.H. Hussein, Investigation of photocatalytic removal and photonic efficiency of maxilon blue dye GRL in the presence of TiO_2 nanoparticles, Part. Sci. Technol., 35 (2017) 14–20.

[9] H.A. Habeeb, S.H. Alwan, Adsorption characteristics of beans peel powder as new adsorbent for Cr(III) removal from aqueous solution, Pharm. Chem., 8 (2016) 42–49.

[10] A.K. Geim, Graphene: status and prospects, Science, 324 (2009) 1530–1534.

[11] S.T. Yang, Y. Chang, H. Wang, G. Liu, S. Chen, Y. Wang, Y. Liu, A. Cao, Folding/aggregation of graphene oxide and its application in Cu^{+2} removal, J. Colloid Interface Sci., 351 (2010) 122–127.

[12] J. Yan, T. Wei, W. Qiao, B. Shao, Q. Zhao, L. Zhang, Z. Fan, Rapid microwave-assisted synthesis of graphene nanosheet/Co_3O_4 composite for supercapacitors, Electrochim. Acta, 55 (2010) 6973–6978.

[13] P. Zong, S. Wang, Y. Zhao, H. Wang, H. Pan, C. He, Synthesis and application of magnetic graphene/iron oxides composite for the removal of U (VI) from aqueous solutions, Chem. Eng. J., 220 (2013) 45–52.

[14] J. Zhao, W. Ren, H.M. Chenga, Graphene sponge for efficient and repeatable adsorption and desorption of water contaminations, J. Mater. Chem., 22 (2012) 20197–20202.

[15] S. Bai, L. Du, J. Sun, R. Luo, D. Li, A. Chen, C.C. Liu, Preparation of reduced graphene oxide/Co_3O_4 composites and sensing performance to toluene at low temperature, RSC Adv., 6 (2016) 60109–60116.

[16] S.D. Perera, R.G. Mariano, K. Vu, N. Nour, O. Seitz, Y. Chabal, K.J. Balkus, Hydrothermal synthesis of graphene-TiO_2 nanotube composites with enhanced photocatalytic activity, ACS Catal., 2 (2012) 949–956.

[17] B. Wang, Y. Wang, J. Park, H. Ahn, G. Wang, In situ synthesis of Co_3O_4/graphene nanocomposite material for lithium-ion batteries and supercapacitors with high capacity and supercapacitance, J. Alloys Compd., 509 (2011) 7778–7783.

[18] S.K. Park, S.H. Yu, N. Pinna, S. Woo, B. Jang, Y.H. Chung, Y.H. Cho, Y.E. Sung, Y. Piao, A facile hydrazine-assisted hydrothermal method for the deposition of monodisperse SnO_2 nanoparticles onto graphene for lithium ion batteries, J. Mater. Chem., 22 (2012) 2520–2525.

[19] W. Zou, J. Zhu, Y. Sun, X. Wang, Depositing ZnO nanoparticles onto graphene in a polyol system, Mater. Chem. Phys., 125 (2011) 617–620.

[20] D. Pathania, G. Sharma, A. Kumar, M. Naushad, S. Kalia, A. Sharma, Z.A. ALOthman, Combined sorptional-photocatalytic remediation of dyes by polyaniline Zr(IV) selenotungstophosphate nanocomposite, Toxicol. Environ. Chem., 97 (2015) 526–537.

[21] S. Xiong, C. Yuan, X. Zhang, B. Xi, Y. Qian, Controllable synthesis of mesoporous Co_3O_4 nanostructures with tunable morphology for application in supercapacitors, Chem. Eur. J., 15 (2009) 5320–5326.

[22] J. Ma, S. Zhang, W. Liu, Y. Zhao, Facile preparation of Co_3O_4 nanocrystals via a solvothermal process directly from common Co_2O_3 powder, J. Alloys Compd., 490 (2010) 647–651.

[23] G. Wang, X. Shen, J. Horvat, B. Wang, H. Liu, D. Wexler, J. Yao, Hydrothermal synthesis and optical, magnetic, and supercapacitance properties of nanoporous cobalt oxide nanorods, J. Phys. Chem. C, 113 (2009) 4357–4361.

[24] L. Yang, W. Guan, B. Bai, Q. Xu, Y. Xiang, Synthesis of yeast-assisted Co_3O_4 hollow microspheres-a novel biotemplating technique, J. Alloys Compd., 504 (2010) L10–L13.

[25] D. Pathania, R. Katwal, G. Sharma, M. Naushad, M. Rizwan Khan, A.H. Al-Muhtaseb, Novel guar gum/Al_2O_3 nanocomposite as an effective photocatalyst for the degradation of malachite green dye, Int. J. Biol. Macromol., 87 (2016) 366–374.

[26] N. Hu, Z. Yang, Y. Wang, L. Zhang, Y. Wang, X. Huang, H. Wei, L. Wei, Y. Zhang, Ultrafast and sensitive room temperature NH_3 gas sensors based on chemically reduced graphene oxide, Nanotechnology, 25 (2013) 025502.

[27] L. Hao, H. Song, L. Zhang, X. Wan, Y. Tang, Y. Lv, SiO_2/graphene composite for highly selective adsorption of Pb (II) ion, J. Colloid Interface Sci., 369 (2012) 381–387.

[28] L. Pan, H. Zhao, W. Shen, X. Dong, J. Xu, Surfactant-assisted synthesis of a Co_3O_4/reduced graphene oxide composite as a superior anode material for Li-ion batteries, J. Mater. Chem. A, 1 (2013) 7159–7166.

[29] P. Shi, R. Su, F. Wan, M. Zhu, D. Li, S. Xu, Co_3O_4 nanocrystals on graphene oxide as a synergistic catalyst for degradation of Orange II in water by advanced oxidation technology based on sulfate radicals, Appl. Catal., B, 123 (2012) 265–272.

[30] Y. Liang, Y. Li, H. Wang, J. Zhou, J. Wang, T. Regier, H. Dai, Co_3O_4 nanocrystals on graphene as a synergistic catalyst for oxygen reduction reaction, Nat. Mater., 10 (2011) 780.

[31] J. Yan, T. Wei, W. Qiao, B. Shao, Q. Zhao, L. Zhang, Z. Fan, Rapid microwave-assisted synthesis of graphene nanosheet/Co_3O_4 composite for supercapacitors, Electrochim. Acta, 55 (2010) 6973–6978.

[32] D.C. Marcano, D.V. Kosynkin, J.M. Berlin, A. Sinitskii, Z. Sun, A. Slesarev, L.B. Alemany, W. Lu, J.M. Tour, Improved synthesis of graphene oxide, Am. Chem. Soc., 4 (2010) 4806–4814.

[33] J. Gao, F. Liu, Y. Liu, N. Ma, Z. Wang, X. Zhang, Environment-friendly method to produce graphene that employs vitamin C and amino acid, Chem. Mater., 22 (2010) 2213–2218.

[34] Q. Yuanchun, Z. Yanbao, W. Zhishen, Preparation of cobalt oxide nanoparticles and cobalt powders by solvothermal process and their characterization, Mater. Chem. Phys., 110 (2008) 457–462.
[35] M. Yarestani, A.D. Khalaji, A. Rohani, D. Das, Hydrothermal synthesis of cobalt oxide nanoparticles: its optical and magnetic properties, J. Sci., Islamic Republic of Iran, 25 (2014) 339–343.
[36] E. Yavuz, Ş. Tokalıoğlu, H. Şahana, Ş. Patata, A graphene/Co_3O_4 nanocomposite as a new adsorbent for solid phase extraction of Pb (II), Cu (II) and Fe (III) ions in various samples, RSC Adv., 3 (2013) 24650–24657.
[37] Y. Li, Q. Du, T. Liu, X. Peng, J. Wang, J. Sun, Y. Wang, S. Wu, Z. Wang, Y. Xia, L. Xia, Comparative study of methylene blue dye adsorption onto activated carbon, graphene oxide, and carbon nanotubes, Chem. Eng. Res. Des., 91 (2013) 361–368.
[38] G. Liu, L. Wang, B. Wang, T. Gao, D. Wang, A reduced graphene oxide modified metallic cobalt composite with superior electrochemical performance for supercapacitors, RSC Adv., 5 (2015) 63553–63560.
[39] Z.S. Wu, W. Ren, L. Wen, L. Gao, J. Zhao, Z. Chen, G. Zhou, F. Li, H.M. Cheng, Graphene anchored with Co_3O_4 nanoparticles as anode of lithium ion batteries with enhanced reversible capacity and cyclic performance, ACS Nano, 4 (2010) 3187–3194.
[40] X. Zhang, K. Li, H. Li, J. Lu, Q. Fu, Y. Chu, Graphene nanosheets synthesis via chemical reduction of graphene oxide using sodium acetate trihydrate solution, Synth. Met., 193 (2014) 132–138.
[41] H.W. Wang, Z.A. Hu, Y.Q. Chang, Y.L. Chen, Z.Y. Zhang, Y.Y. Yang, H.Y. Wu, Preparation of reduced graphene oxide/cobalt oxide composites and their enhanced capacitive behaviors by homogeneous incorporation of reduced graphene oxide sheets in cobalt oxide matrix, Mater. Chem. Phys., 130 (2011) 672–679.
[42] D. Chen, L. Li, L. Guo, An environment-friendly preparation of reduced graphene oxide nanosheets via amino acid, Nanotechnology, 22 (2011) 325601.
[43] Y. Zhang, H.L. Ma, Q. Zhang, J. Peng, J. Li, M. Zhai, Z.Z. Yu, Facile synthesis of well-dispersed graphene by γ-ray induced reduction of graphene oxide, J. Mater. Chem., 22 (2012) 13064–13069.
[44] S. Farhadi, K. Pourzare, S. Bazgir, Co_3O_4 nanoplates: synthesis, characterization and study of optical and magnetic properties, J. Alloys Compd., 587 (2014) 632–637.
[45] X. Yang, K. Fan, Y. Zhu, J. Shen, X. Jiang, P. Zhao, C. Li, Tailored graphene-encapsulated mesoporous Co_3O_4 composite microspheres for high-performance lithium ion batteries, J. Mater. Chem., 22 (2012) 17278–17283.
[46] A.B. Albadarin, M. Charara, B.J. Abu Tarboush, M.N.M. Ahmad, T.A. Kurniawan, M. Naushad, G.M. Walker, C. Mangwandi, Mechanism analysis of tartrazine biosorption onto masau stones; a low cost by-product from semi-arid regions, J. Mol. Liq., 242 (2017) 478–483.
[47] S.Y. Toh, K.S. Loh, S.K. Kamarudin, W.R.W. Daud, Graphene production via electrochemical reduction of graphene oxide: synthesis and characterisation, Chem. Eng. J., 251 (2014) 422–434.
[48] K. Agilandeswari, A.R. Kumar, Synthesis, characterization and optical properties of Co_3O_4 by precipitation method, Int. J. ChemTech Res., 6 (2014) 2089–2092.
[49] E. Daneshvar, A. Vazirzadeh, A. Niazi, M. Kousha, M. Naushad, A. Bhatnagar, Desorption of methylene blue dye from brown macroalga: effects of operating parameters, isotherm study and kinetic modeling, J. Cleaner Prod., 152 (2017) 443–453.
[50] G. Wang, B. Wang, J. Park, J. Yang, X. Shen, J. Yao, Synthesis of enhanced hydrophilic and hydrophobic graphene oxide nanosheets by a solvothermal method, Carbon, 47 (2009) 68–72.
[51] P. Song, X. Zhang, M. Sun, X. Cui, Y. Lin, Synthesis of graphene nanosheets via oxalic acid-induced chemical reduction of exfoliated graphite oxide, RSC Adv., 2 (2012) 1168–1173.
[52] T. Ozkaya, A. Baykal, Y. Koseoğlu, H. Kavas, Synthesis of Co_3O_4 nanoparticles by oxidation-reduction method and its magnetic characterization, Open Chem., 7 (2009) 410–414.
[53] Y. Haldorai, J.Y. Kim, A.T.E. Vilian, N.S. Heo, Y.S. Huh, Y.K. Han, An enzyme-free electrochemical sensor based on reduced graphene oxide/Co_3O_4 nanospindle composite for sensitive detection of nitrite, Sens. Actuators, B, 227 (2016) 92–99.
[54] Y. Zhao, S. Chen, B. Sun, D. Su, X. Huang, H. Liu, Y. Yan, K. Sun, G. Wang, Graphene-Co_3O_4 nanocomposite as electrocatalyst with high performance for oxygen evolution reaction, Sci. Rep., 5 (2015) 7629.
[55] I. Jung, D.A. Dikin, R.D. Piner, R.S. Ruoff, Tunable electrical conductivity of individual graphene oxide sheets reduced at "low" temperatures, Nano Lett., 8 (2008) 4283–4287.
[56] G. Goncalves, P.A.A.P. Marques, C.M. Granadeiro, H.I.S. Nogueira, M.K. Singh, J. Grácio, Surface modification of graphene nanosheets with gold nanoparticles: the role of oxygen moieties at graphene surface on gold nucleation and growth, Chem. Mater., 21 (2009) 4796–4802.
[57] B.G. Choi, S.J. Chang, Y.B. Lee, J.S. Bae, H.J. Kim, Y.S. Huh, 3D heterostructured architectures of Co_3O_4 nanoparticles deposited on porous graphene surfaces for high performance of lithium ion batteries, Nanoscale, 4 (2012) 5924–5930.
[58] Y. Zhuang, F. Yu, J. Ma, J. Chen, Adsorption of ciprofloxacin onto graphene-soy protein biocomposites, New J. Chem., 39 (2015) 3333–3336.
[59] P. Banerjee, P. Das, A. Zaman, P. Das, Application of graphene oxide nanoplatelets for adsorption of ibuprofen from aqueous solutions: evaluation of process kinetics and thermodynamics, Process Saf. Environ. Prot., 101 (2016) 45–53.
[60] G. Sharma, M. Naushad, A.H. Al-Muhtaseb, A. Kumar, M.R. Khan, S. Kalia, Shweta, M. Bala, A. Sharma, Fabrication and characterization of chitosan-crosslinked-poly(alginic acid) nanohydrogel for adsorptive removal of Cr(VI) metal ion from aqueous medium, Int. J. Biol. Macromol., 95 (2017) 484–493.
[61] H.B. Senturk, D. Ozdes, C. Duran, Biosorption of Rhodamine 6G from aqueous solutions onto almond shell (*Prunus dulcis*) as a low cost biosorbents, Desalination, 252 (2010) 81–87.
[62] Y. Gao, Y. Li, L. Zhang, H. Huang, J. Hu, S.M. Shah, X. Su, Adsorption and removal of tetracycline antibiotics from aqueous solution by graphene oxide, J. Colloid Interface Sci., 368 (2012) 540–546.
[63] P. Banerjee, S. Sau, P. Das, A. Mukhopadhayay, Optimization and modelling of synthetic azo dye wastewater treatment using graphene oxide nanoplatelets: characterization toxicity evaluation and optimization using artificial neural network, Ecotoxicol. Environ. Saf., 119 (2015) 47–57.
[64] H. Wang, X. Yuan, Y. Wu, H. Huang, G. Zeng, Y. Liu, X. Wang, N. Lin, Y. Qi, Adsorption characteristics and behaviors of graphene oxide for Zn (II) removal from aqueous solution, Appl. Surf. Sci., 279 (2013) 432–440.
[65] L. Ji, W. Chen, J. Bi, S. Zheng, Z. Xu, D. Zhu, P.J. Alvarez, Adsorption of tetracycline on single-walled and multi-walled carbon nanotubes as affected by aqueous solution chemistry, Environ. Toxicol. Chem., 29 (2010) 2713–2719.